Scaling density of axion strings

Article (Accepted Version)

The scaling density of axion strings

Mark Hindmarsh,[1, 2, *] Joanes Lizarraga,[3, †] Asier Lopez-Eiguren,[1, ‡] and Jon Urrestilla[3, §]

[1] *Department of Physics and Helsinki Institute of Physics, PL 64, FI-00014 University of Helsinki, Finland*
[2] *Department of Physics and Astronomy, University of Sussex, Falmer, Brighton BN1 9QH, U.K.*
[3] *Department of Theoretical Physics, University of the Basque Country UPV/EHU, 48080 Bilbao, Spain*

(Dated: August 4, 2020)

In the QCD axion dark matter scenario with post-inflationary Peccei-Quinn symmetry breaking, the number density of axions, and hence the dark matter density, depends on the length of string per unit volume at cosmic time t, by convention written ζ/t^2. The expectation has been that the dimensionless parameter ζ tends to a constant ζ_0, a feature of a string network known as scaling. It has recently been claimed that in larger numerical simulations ζ shows a logarithmic increase with time, while theoretical modelling suggests an inverse logarithmic correction. Either case would result in a large enhancement of the string density at the QCD transition, and a substantial revision to the axion mass required for the axion to constitute all of the dark matter. With a set of new simulations of global strings we compare the standard scaling (constant-ζ) model to the logarithmic growth and inverse-logarithmic correction models. In the standard scaling model, by fitting to linear growth in the mean string separation $\xi = t/\sqrt{\zeta}$, we find $\zeta_0 = 1.19 \pm 0.20$. We conclude that the apparent corrections to ζ are artefacts of the initial conditions, rather than a property of the scaling network. The residuals from the constant-ζ (linear ξ) fit also show no evidence for logarithmic growth, restoring confidence that numerical simulations can be simply extrapolated from the Peccei-Quinn symmetry-breaking scale to the QCD scale. Re-analysis of previous work on the axion number density suggests that recent estimates of the axion dark matter mass in the post-inflationary symmetry-breaking scenario we study should be increased by about 50%.

Introduction: The Peccei-Quinn (PQ) mechanism, which solves the strong CP problem of QCD by extending the Standard Model with an extra U(1) global symmetry [1], brings with it a long-lived pseudoscalar particle, the axion [2]. A universe where light axions [3, 4] constitute the dark matter [5] is one of the most promising scenarios in the current cosmological paradigm.

If the PQ symmetry is spontaneously broken after primordial inflation, axion strings are formed [6], a variety of global cosmic string [7, 8]. They survive until the QCD confinement transition, when they become connected by domain walls made of the CP-odd gluon condensate [9, 10], and are annihilated. Most of the energy is left behind in the form of axion radiation, produced through the lifetime of the string network and during the annihilation phase. The axion radiation can also be viewed as light massive particles, whose number density depends on the length of string per unit volume ζ/t^2, where t is cosmic time. The important dimensionless parameter ζ can be established only by numerical simulations.

The usual expectation (see [11–13]) is that the string density parameter ζ converges to a constant within a few Hubble times after the network is formed, part of a wider assumption known as scaling. Scaling means that the string network is statistically self-similar; *i.e.* all macroscopic quantities with the dimensions of length and time are proportional to the Hubble length and time. Earlier simulations of global cosmic strings [14–21] were consistent with scaling with $\zeta \sim 1$, and there is good theoretical understanding of scaling from modelling the global properties of the network [22, 23].

However, several groups have recently claimed that ζ shows a logarithmic increase with time [24–27]. An argument for expecting a scaling violation is based on the logarithmic growth in the effective string tension of a global string with their mean separation. If there is no corresponding change in the energy loss rate per unit length, the string length density parameter should grow [28–31].

In fact this argument does not lead to logarithmic growth of ζ; instead it gives a leading correction to scaling of an inverse logarithm [32]. Nonetheless, either behaviour would lead to a larger asymptotic string density parameter, which would lead to an increase of the axion number density, and hence a decrease in the axion mass required to match the current dark matter mass density.

In this work we present results from a new set of numerical simulations of global strings. We explore the effect of different initial string densities and lattice sizes. We compare the results for the string density in three different two-parameter models defined below: standard scaling, logarithmic, and inverse-logarithmic. We demonstrate that all simulations are consistent with standard scaling, and determine the asymptotic string length density parameter ζ_0 to the best precision to date.

We conclude that the axion string density shows excellent scaling following the PQ phase transition, justifying a constant-ζ extrapolation to the QCD transition. We re-examine previous results to see how estimates of the axion number density, and hence the axion dark matter mass, are affected.

Model and Simulations: The simplest axion models [3, 4] break the $\mathrm{U(1)_{PQ}}$ symmetry with a scalar gauge singlet field, which we can write as a real scalar doublet

Φ with action

$$S = \int d^4x\sqrt{-g}\Big(\frac{1}{2}\partial_\mu\Phi\partial^\mu\Phi - \frac{1}{4}\lambda(\Phi^2-\eta^2)^2\Big), \qquad (1)$$

where λ is the self-coupling of the scalar field and η its vacuum expectation value. The metric $g_{\mu\nu}$ is the spatially flat Friedmann-Lemaître-Robertson-Walker metric with comoving spatial coordinates $ds^2 = dt^2 - a^2(t)d\boldsymbol{r}^2$, where $a(t)$ is the scale factor and t is physical time.

When PQ symmetry is spontaneously broken, axion strings are formed and one massless Goldstone boson and one massive boson arise. Even though the axions acquire a small mass, when the coupling to QCD fields are considered [1], at high temperatures the axion mass can be neglected, and the field obeys the following dynamics:

$$\Phi'' + 2\frac{a'}{a}\Phi' - \nabla^2\Phi = -a^2\lambda(\Phi^2-\eta^2)\Phi, \qquad (2)$$

where the primes represent derivatives with respect to the conformal time $\tau = \int dt a^{-1}(t)$. For axion string evolution, $a \propto \tau$.

The evolution of the field is simulated with a discretised version of Eq. (2), parallelised using the LATfield2 library [33]. We use cubic lattices with periodic boundary conditions, which impose an upper limit in the dynamical range of the simulation of half a light-crossing time, beyond which it is possible for the Goldstone modes to show finite volume effects in their propagation. Note that we do not use the Press-Ryden-Spergel method [34]; data is taken while the string core has constant physical width $r_{\rm s} = m_{\rm s}^{-1}$ and shrinking comoving width.

We use initial conditions designed to drive the system quickly to scaling. To this end, a satisfactory initial field configuration is given by the scalar field velocities $\dot{\Phi}$ set to zero and the components of Φ to be Gaussian random fields with power spectrum, $P_\Phi(\mathbf{k}) = A\left[1+(k\ell_\phi)^2\right]^{-1}$, with A chosen so that $\langle\Phi^2\rangle = \eta^2$. We use comoving correlation lengths $\ell_\phi\eta = (5, 10, 20)$. We run with lattice sites per side $N = [1k, 2k, 4k]$ (where $k = 1024$), and perform 4 independent runs in each different lattice and for each correlation length.

In order to remove energy from the initial configuration, λ is time-dependent in the preparation phase, so that we can arrange $m_{\rm s}a \simeq 2\eta$ at $\tau_{\rm ini}\eta = 50$, and apply a period of diffusive evolution with unit diffusion constant, until $\tau_{\rm diff}\eta = 70$. We then apply the second order equations (2), allowing the comoving width of the strings to grow to their physical value at $\tau_{\rm cg}\eta = [144.9, 196.2, 271.1]$ for $N = [1k, 2k, 4k]$.

The physical evolution begins at $\tau_{\rm cg}$ and ends at $\tau_{\rm end}\eta = [300, 550, 1050]$, when $m_s a = 2\eta$, during which $\lambda = 2$ is constant. We normalise the scale factor so that $a(\tau_{\rm end}) = 1$. The comoving lattice spacing is $\delta x\eta = 0.5$, the conformal timestep during diffusion is $\delta\tau = \delta x/30$ and during second order evolution $\delta\tau = \delta x/5$. In the subsequent figures and tables the unit of length is η^{-1}.

Measurements and results: The evolution of the string network can be tracked by the mean string separation ξ, defined in terms of the mean string length $\ell_{\rm s}$ in the simulation volume $\mathcal{V}$ as

$$\xi = \sqrt{\mathcal{V}/\ell_{\rm s}}. \qquad (3)$$

The physical string length ℓ_s is the number of plaquettes pierced by strings multiplied by the physical lattice spacing $a\delta x$, corrected by factor of 2/3 to compensate for the Manhattan effect [28]. Such plaquettes are identified calculating the "winding" of the phase of the field around each plaquette of the lattice [35].

A dimensionless measure of the length of string per unit volume [8, 24–26, 30, 32] is

$$\zeta = \ell_{\rm s}t^2/\mathcal{V} = t^2/\xi^2, \qquad (4)$$

which in a radiation-dominated universe is four times the number of Hubble lengths of string per Hubble volume (note that some authors use ξ to denote this quantity).

As there is no fixed length scale in the string equations of motion, string networks are expected to evolve towards a self-similar or scaling regime, in which the only length scale is t [7, 8, 22]. Hence ξ should increase linearly with time, and ζ should evolve towards a constant. However, the formation and initial evolution of the network introduces a time scale, which can be taken to be the t-axis intercept of a linear fit to $\xi(t)$ [36]. We call this the initial string evolution parameter, and denote it t_0. Over cosmological timescales the ratio $t_0/t \to 0$; however, in numerical simulations it must be taken into account when extracting the scaling value of ζ, which we denote ζ_0.

Fig. 1 shows the results for the mean string separation ξ for $4k$ simulations with different initial correlation lengths. Graphs of ξ against t for all runs are shown in the Supplemental Material. Consistent with our earlier simulations [21], after a relatively short period of relaxation, ξ asymptotes to a line that can be well fitted with[1]

$$\xi = 2\beta(t - t_0). \qquad (5)$$

This is the standard scaling model. The scaling value of the length density parameter is $\zeta_0 = 1/4\beta^2$.

We measure the parameters β and t_0 with a linear fit over four ranges in conformal time, defined by a vector of boundary times $\tau_{\rm b} = (6, 7, 8, 9, 10)\tau_s$, and $\tau_s\eta = [25, 50, 100]$ for $N = [1k, 2k, 4k]$. We choose times in the last half of the conformal time range to minimise

[1] Note that β as defined here is the slope of the comoving string separation ξ/a plotted against conformal time $\tau = 2t/a$.

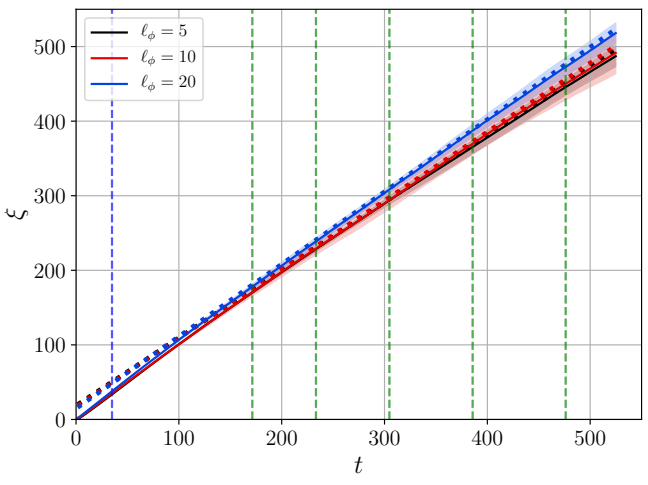

FIG. 1. Mean string separation ξ (defined in Eq. (3)) from 4k simulations with all initial field correlation lengths ℓ_ϕ. The solid line represents the mean over realizations of ξ at each time, with the shaded regions showing the 1-σ variation. Also shown as dotted lines are the linear fits to the form of Eq. (5), whose parameters and uncertainties are shown in Table I. The blue vertical dashed line is the end of the core growth period ($t_{\rm cg}$), after which strings maintain their physical width, and the green ones are the boundaries of the fitting ranges.

biases from the initial conditions. The standard deviation of the central values of the parameters in the different fit ranges can be used to give an estimate of the combined uncertainty due to the approach to scaling and the lattice spacing: later fits will be closer to the scaling value, but more affected by the lattice spacing, which is equal to the inverse mass $(2\eta)^{-1}$ at the end of the simulation. The standard deviation of the central values between different ℓ_ϕ gives an estimate of the uncertainty due to the initial correlation length. The two uncertainties are added in quadrature to give an estimate of the systematic error $\Delta\beta_{\rm sys}$, which is dominated by the uncertainty due to the variation in initial correlation lengths. The total uncertainty is obtained from adding the statistical and systematic uncertainties in quadrature. The means and uncertainties for the standard scaling parameters can be found in Tables I and II.

We now turn to the alternative models recently put forward: logarithmic [24–27], and inverse logarithmic [32] correction to scaling

$$\zeta(t) = \zeta_0^* + \alpha^* \log(\eta t), \quad \zeta(t) = \zeta_0' + \alpha'/\log(\eta t), \qquad (6)$$

where ζ_0^*, ζ_0', α^* and α' are the fitting parameters. We performed fits over the four ranges used previously, using the same method to estimate uncertainties. The mean values and uncertainties for the parameters can be found in Table III.

The uncertainties include zero, and are apparently inconsistent with reports of a logarithmic correction with

$\Delta t_{\rm fit}$	ℓ_ϕ	t_0	β	ζ_0
171.42 - 233.33	5	-8.94 ± 2.74	0.47 ± 0.01	1.12 ± 0.05
171.42 - 233.33	10	-7.48 ± 8.47	0.48 ± 0.03	1.11 ± 0.15
171.42 - 233.33	20	-10.00 ± 1.81	0.49 ± 0.01	1.04 ± 0.05
233.33 - 304.76	5	-16.46 ± 10.27	0.46 ± 0.02	1.20 ± 0.11
233.33 - 304.76	10	-19.64 ± 4.54	0.45 ± 0.02	1.22 ± 0.13
233.33 - 304.76	20	-12.59 ± 13.29	0.49 ± 0.02	1.06 ± 0.09
304.76 - 385.71	5	-29.83 ± 11.13	0.44 ± 0.02	1.30 ± 0.13
304.76 - 385.71	10	-12.32 ± 20.42	0.47 ± 0.03	1.16 ± 0.16
304.76 - 385.71	20	-12.93 ± 15.52	0.49 ± 0.03	1.07 ± 0.12
385.71 - 476.19	5	-27.32 ± 27.07	0.44 ± 0.03	1.28 ± 0.17
385.71 - 476.19	10	-34.48 ± 39.63	0.45 ± 0.05	1.31 ± 0.31
385.71 - 476.19	20	-23.79 ± 16.37	0.47 ± 0.03	1.12 ± 0.13

TABLE I. Numerical values of the fit parameters for the 4k runs fitted over the conformal time ranges given after Eq. (5), shown in physical time as $\Delta t_{\rm fit}$. The fit parameters t_0 and β pertain to Eq. (5), with $\zeta_0 = 1/4\beta^2$. The values are computed averaging over the 4 different realisations and the computation of the uncertainties is described after Eq. (5).

N	$\beta \pm \Delta\beta$	$\Delta\beta_{\rm stat}$	$\Delta\beta_{\rm sys}$	$\zeta_0 \pm \Delta\zeta_0$	$\Delta\zeta_{0,\rm stat}$	$\Delta\zeta_{0,\rm sys}$
$1k$	0.499 ± 0.042	0.031	0.028	1.02 ± 0.17	0.13	0.11
$2k$	0.486 ± 0.036	0.030	0.019	1.07 ± 0.16	0.13	0.08
$4k$	0.467 ± 0.037	0.030	0.021	1.17 ± 0.20	0.17	0.11

TABLE II. Central values and estimated uncertainties of the standard scaling parameters β and $\zeta_0 = 1/4\beta^2$ for all box sizes. The decomposition into statistical and systematic uncertainties, as discussed in the text after Eq. (5), is also shown.

coefficient $\alpha^* \simeq 0.2$ [24, 25]. It is interesting to examine why. If the strings are scaling in the sense that the mean string separation ξ is increasing linearly, the string density parameter ζ behaves as

$$\zeta = \frac{t^2}{4\beta^2(t-t_0)^2} \simeq \zeta_0\left(1 + 2\frac{t_0}{t}\right). \qquad (7)$$

The uncorrected estimator approaches its asymptotic value slowly, resembling the behaviour of a logarithm with a positive coefficient,

$$\alpha^*(t_f) = -2\zeta(t_0/t_f)(1 - t_0/t_f)^{-1}, \qquad (8)$$

where t_f is a time at which the fit is carried out. We find that taking t_f to be the final time in the fit range gives the best fit. If $t_0 < 0$, the approach is from lower ("underdense") values of ζ, giving positive values of α^*, and vice versa. Hence an apparent logarithmic growth parameter $\alpha^* \simeq 0.2$ [24, 25] is produced for runs where the initial string configurations are biased towards $t_0/t_f \simeq -0.1$. Our initial conditions cover both positive and negative values of α^*, and are consistent with $\alpha^* = 0$ as $t_0/t_f \to 0$. The parameter α' similarly takes both signs and is consistent with zero as $t_0/t_f \to 0$. The constant terms in the alternative models are consistent with standard scaling $\zeta_0^*, \zeta_0' \simeq 1$ as $t_0/t_f \to 0$. The standard scaling parameter β depends only weakly on t_0/t_f. This effect is included in

N	ζ_0^*	α^*	ζ_0'	α'	ζ_r $(\times 10^{-2})$	α_r $(\times 10^{-2})$
$1k$	1.7 ± 1.0	-0.14 ± 0.21	0.55± 0.69	2.4± 3.3	0.0 ± 1.3	-0.02 ± 0.31
$2k$	0.88 ± 0.60	0.03 ± 0.11	1.18 ± 0.58	-0.8 ± 3.0	0.2 ± 1.6	-0.04 ± 0.33
$4k$	0.42 ± 0.59	0.11 ± 0.11	1.66 ± 0.68	-3.6 ± 3.8	0.2 ± 1.5	-0.03 ± 0.26

TABLE III. Numerical values of the fit parameters of the logarithmic correction, inverse logarithmic correction, and residuals as presented in Eqs. (6) and (10) respectively. Fitting ranges and error estimates were obtained following the same prescription as in the previous tables.

our uncertainty, and is smaller than the statistical fluctuations. More information is given in the Supplemental Material.

We also explore the possibility of a small drift away from standard scaling in the residuals, by using the length density parameter estimator

$$\hat{\zeta} = \ell_s (t - t_0)^2 / \mathcal{V} = (t - t_0)^2 / \xi^2 \,, \tag{9}$$

where t_0 is the best fit value from the fit (5) for $\xi(t)$. In Fig. 2 we plot $\hat{\zeta}$ against $t - t_0$ for the 4 runs with $\ell_\phi \eta = 5$. The figure gives a clear impression of $\hat{\zeta}$ tending to an asymptotically constant value. The residuals to the standard scaling fit for $\ell_\phi \eta = 5$ are also shown in Fig. 2, with the mean shown as a dashed line. We fit the residual to a constant plus a logarithm according to

$$\hat{\zeta}(t) - \zeta_0 = \zeta_{\rm r} + \alpha_{\rm r} \log(\eta t), \tag{10}$$

where $\alpha_{\rm r}$ and $\zeta_{\rm r}$ are fitting parameters, fitted over the four ranges in conformal time described earlier.

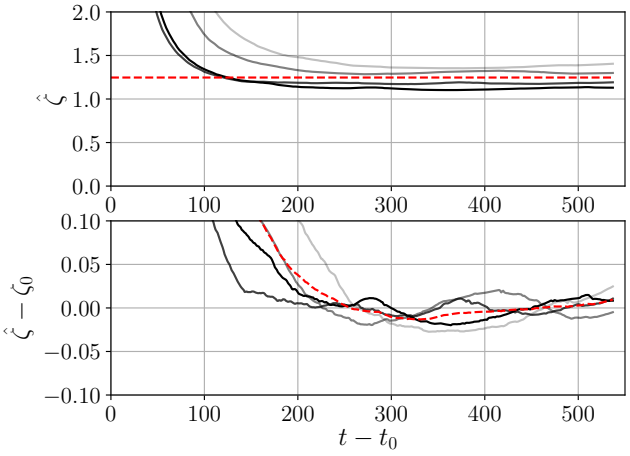

FIG. 2. Top: string length density parameter $\hat{\zeta}$ (see Eq. (5)) plotted against offset time $t - t_0$, for all $4k$ runs with initial correlation length $\ell_\phi = 5$. The dashed line shows the mean of $\zeta_0 = 1/4\beta^2$. Bottom: residuals $(\hat{\zeta} - \zeta_0)$ plotted against offset time $t - t_0$, for the same simulations. Individual runs are showed in solid lines and the residuals between the mean ζ_0 and $\hat{\zeta}$ in dashed.

The measured values of $\zeta_{\rm r}$ and $\alpha_{\rm r}$ are given in Table III, along with the uncertainties. They are consistent with zero, and give a tight bound on any logarithmic growth in the string length density parameter in the residual.

Having determined that standard scaling is the best model, we explore the uncertainty due to the finite lattice volume. We average the fit parameters over initial correlation lengths and fit ranges at each lattice size, and then perform a linear extrapolation in $1/L\eta$. Our final result for the length density parameter is[2]

$$\zeta_0 = 1.19 \pm 0.20. \tag{11}$$

The coefficient of any logarithm in the residuals is

$$\alpha_{\rm r} = (-0.04 \pm 0.30) \times 10^{-2}, \tag{12}$$

consistent with zero. The dominant error is statistical.

Conclusions: In this paper we have investigated the scaling density of axion strings, prompted by recent claims of a logarithmic increase in the string length density parameter ζ [24–30].

We have fitted the string length density from our simulations with three two-parameter models: the standard scaling model with the usual time offset t_0 to account for the initial string evolution and an asymptotically constant length density parameter ζ_0; a model with a logarithmically increasing ζ; and a model with an inverse logarithmic correction. By linear fits to the mean string separation ξ, we obtain a well-determined result for the parameter ζ_0, given in Eq. (11). The coefficients of the logarithm and inverse logarithm can be understood in terms of the dependence of ζ on the initial string evolution parameter t_0, and describe a disguised approach to scaling for non-zero t_0. We find they are consistent with zero when $t_0/t_f \to 0$, where t_f is the final fitting time. The constant terms in the models consistent with the standard scaling values. A search for a logarithmic correction to the residuals of the standard scaling model gives a tight upper bound on the magnitude of its coefficient (12): our 3σ limit on a logarithmic correction to the string density parameter is $|\alpha| < 0.94 \times 10^{-2}$.

We conclude that axion strings scale very well in the standard sense, and that between a 10^{12} GeV PQ phase transition and the QCD transition at 100 MeV, any logarithmic correction to the string density parameter $\zeta_0 \simeq 1$ must be less than about 0.5.

An implication of the confirmation of standard scaling, important for network modelling [32], is that the energy loss rate per unit length of string must increase at the same rate as the effective string tension.

The tight constraint on the logarithmic correction also has implications for attempts to extend the dynamic

[2] We have also performed simulation with constant comoving width, and observe a similar behaviour, with $\zeta_0 = 1.34 \pm 0.22$. See the Supplemental Material.

range of global string simulations [28–30] by using frustrated strings [31]. Frustrated string models have fields with both global and local symmetries, and the string resembles a global string with an Abelian Higgs string at the core. The effect is to decouple the string tension μ and the axion decay constant $f_{\rm a}$, so that $\kappa = \mu/\pi f_{\rm a}^2$ can be chosen to be greater than 1. As the effective tension of an axion string is $\mu_{\rm a} \simeq \pi f_{\rm a}^2 \ln(\xi\eta)$, it was argued that a simulation with frustrated strings would effectively reach a string separation $\xi \sim \eta^{-1}\exp(\kappa)$.

It was found that there was an increase in the length density parameter ζ with the ratio $\kappa = \mu/\pi f_{\rm a}^2$, apparently saturating at $\zeta \simeq 20$ around $\kappa \simeq 50$ [30]. This is far above our O(1) upper bound on ζ at the QCD scale, casting doubt on the effectiveness of frustrated strings as a generic model of axion strings at large separations. Hence one should not extrapolate the axion number density $n_{\rm ax}$ to $\kappa \sim 70$. From Fig. 6 (right) of Ref. [30] one can estimate that $n_{\rm ax}/n_{\rm mis} \simeq 0.5$ at $\kappa = 1$, where $n_{\rm mis}$ is the angle-averaged number density produced by the misalignment mechanism [5, 30, 37–39]. This is consistent with the directly-measured values reported by other groups [20, 26]. This value is about 60% of the extrapolated value [30], suggesting that the value of the axion dark matter mass of about 25 μeV [30] should be revised upwards by about 50% in scenarios based on PQ symmetry-breaking by a gauge singlet. We leave a more precise estimate for future work.

Finally, we note that frustrated string models [28–30] may be viable if the PQ symmetry-breaking is accompanied by the breaking of a U(1) gauge symmetry. The difference in the axion dark matter mass estimates between the models implies that the detection of an axion and an accurate measurement of its mass could distinguish between them.

We are grateful for fruitful discussions with M. Kawasaki, J. Redondo, K. Saikawa, T. Sekiguchi, G. Villadoro, M. Yamaguchi and J. Yokoyama. MH (ORCID ID 0000-0002-9307-437X) acknowledges support from the Science and Technology Facilities Council (grant number ST/L000504/1). JL (ORCID ID 0000-0002-1198-3191) and JU (ORCID ID 0000-0002-4221-2859) acknowledge support from Eusko Jaurlaritza (IT-979-16) and PGC2018-094626-B-C21 (MCIU/AEI/FEDER,UE). ALE (ORCID ID 0000-0002-1696-3579) is supported by the Academy of Finland grant 286769. ALE is grateful to the Early Universe Cosmology group of the University of the Basque Country for their generous hospitality and useful discussions. This work has been possible thanks to the computational resources on the STFC DiRAC HPC facility obtained under the dp116 project. Our simulations also made use of facilities at the i2Basque academic network and CSC Finland.

* mark.hindmarsh@helsinki.fi
† joanes.lizarraga@ehu.eus
‡ asier.lopezeiguren@helsinki.fi
§ jon.urrestilla@ehu.eus

[1] R. D. Peccei and H. R. Quinn, Phys. Rev. Lett. **38**, 1440 (1977)Phys. Rev. **D16**, 1791 (1977)
[2] S. Weinberg, Phys. Rev. Lett. **40**, 223 (1978)F. Wilczek, **40**, 279 (1978)
[3] J. E. Kim, Phys. Rev. Lett. **43**, 103 (1979)M. A. Shifman, A. I. Vainshtein, and V. I. Zakharov, Nucl. Phys. **B166**, 493 (1980)
[4] A. R. Zhitnitsky, Sov. J. Nucl. Phys. **31**, 260 (1980), [Yad. Fiz.31,497(1980)]M. Dine, W. Fischler, and M. Srednicki, Phys. Lett. **104B**, 199 (1981)
[5] J. Preskill, M. B. Wise, and F. Wilczek, Phys. Lett. **B120**, 127 (1983)L. F. Abbott and P. Sikivie, **B120**, 133 (1983)M. Dine and W. Fischler, **B120**, 137 (1983)
[6] R. L. Davis, Phys. Lett. **B180**, 225 (1986)
[7] M. Hindmarsh and T. Kibble, Rept.Prog.Phys. **58**, 477 (1995), arXiv:hep-ph/9411342 [hep-ph]
[8] A. Vilenkin and E. P. S. Shellard, *Cosmic Strings and Other Topological Defects* (Cambridge University Press, 2000) ISBN 9780521654760, `http://www.cambridge.org/mw/academic/subjects/physics/theoretical-physics-and-mathematical-physics/cosmic-strings-and-other-topological-defects?format=PB`
[9] P. Sikivie, Phys. Rev. Lett. **48**, 1156 (1982)
[10] H. Georgi and M. B. Wise, Phys. Lett. **116B**, 123 (1982)
[11] E. P. S. Shellard and R. A. Battye, *Sources and detection of dark matter in the universe. Proceedings, 3rd International Symposium, and Workshop on Primordial Black Holes and Hawking Radiation, Marina del Rey, USA, February 17-20, 1998*, Phys. Rept. **307**, 227 (1998), arXiv:astro-ph/9808220 [astro-ph]
[12] P. Sikivie, *Axions: Theory, cosmology, and experimental searches. Proceedings, 1st Joint ILIAS-CERN-CAST axion training, Geneva, Switzerland, November 30-December 2, 2005*, Lect. Notes Phys. **741**, 19 (2008), [,19(2006)], arXiv:astro-ph/0610440 [astro-ph]
[13] J. E. Kim and G. Carosi, Rev. Mod. Phys. **82**, 557 (2010), arXiv:0807.3125 [hep-ph]
[14] M. Yamaguchi, M. Kawasaki, and J. Yokoyama, Phys. Rev. Lett. **82**, 4578 (1999), arXiv:hep-ph/9811311 [hep-ph]
[15] M. Yamaguchi, M. Kawasaki, and J. Yokoyama, in *Proceedings, 7th International Symposium on Particles, Strings and Cosmology (PASCOS 99): Lake Tahoe, California, December 10-16, 1999* (1999) pp. 291–294
[16] M. Yamaguchi, M. Kawasaki, and J. Yokoyama, in *Proceedings, 3rd International Workshop on The identification of dark matter (IDM 2000): York, UK, September 18-22, 2000* (2000) pp. 297–304
[17] M. Yamaguchi and J. Yokoyama, Phys. Rev. **D67**, 103514 (2003), arXiv:hep-ph/0210343 [hep-ph]
[18] T. Hiramatsu, M. Kawasaki, T. Sekiguchi, M. Yamaguchi, and J. Yokoyama, Phys. Rev. **D83**, 123531 (2011), arXiv:1012.5502 [hep-ph]
[19] T. Hiramatsu, M. Kawasaki, K. Saikawa, and T. Sekiguchi, Phys. Rev. **D85**, 105020 (2012), [Erratum: Phys. Rev.D86,089902(2012)], arXiv:1202.5851 [hep-ph]

[20] M. Kawasaki, K. Saikawa, and T. Sekiguchi, Phys. Rev. **D91**, 065014 (2015), arXiv:1412.0789 [hep-ph]
[21] A. Lopez-Eiguren, J. Lizarraga, M. Hindmarsh, and J. Urrestilla, JCAP **1707**, 026 (2017), arXiv:1705.04154 [astro-ph.CO]
[22] C. J. A. P. Martins and E. P. S. Shellard, Phys. Rev. **D54**, 2535 (1996), arXiv:hep-ph/9602271 [hep-ph]
[23] C. Martins and E. Shellard, Phys.Rev. **D65**, 043514 (2002), arXiv:hep-ph/0003298 [hep-ph]
[24] M. Gorghetto, E. Hardy, and G. Villadoro, JHEP **07**, 151 (2018), arXiv:1806.04677 [hep-ph]
[25] M. Kawasaki, T. Sekiguchi, M. Yamaguchi, and J. Yokoyama, PTEP **2018**, 091E01 (2018), arXiv:1806.05566 [hep-ph]
[26] A. Vaquero, J. Redondo, and J. Stadler, JCAP **1904**, 012 (2019), arXiv:1809.09241 [astro-ph.CO]
[27] M. Buschmann, J. W. Foster, and B. R. Safdi(2019), arXiv:1906.00967 [astro-ph.CO]
[28] L. Fleury and G. D. Moore, JCAP **1601**, 004 (2016), arXiv:1509.00026 [hep-ph]
[29] V. B. Klaer and G. D. Moore, JCAP **1710**, 043 (2017), arXiv:1707.05566 [hep-ph]
[30] V. B. Klaer and G. D. Moore, JCAP **1711**, 049 (2017), arXiv:1708.07521 [hep-ph]
[31] C. T. Hill, A. L. Kagan, and L. M. Widrow, Phys. Rev. **D38**, 1100 (1988)
[32] C. J. A. P. Martins, Phys. Lett. **B788**, 147 (2019), arXiv:1811.12678 [astro-ph.CO]
[33] D. Daverio, M. Hindmarsh, and N. Bevis, ArXiv e-prints(2015), arXiv:1508.05610 [physics.comp-ph]
[34] W. H. Press, B. S. Ryden, and D. N. Spergel, Astrophys. J. **347**, 590 (1989)
[35] T. Vachaspati and A. Vilenkin, Phys. Rev. **D30**, 2036 (1984)
[36] N. Bevis, M. Hindmarsh, M. Kunz, and J. Urrestilla, Phys.Rev. **D82**, 065004 (2010), arXiv:1005.2663 [astro-ph.CO]
[37] K. J. Bae, J.-H. Huh, and J. E. Kim, JCAP **0809**, 005 (2008), arXiv:0806.0497 [hep-ph]
[38] O. Wantz and E. P. S. Shellard, Phys. Rev. **D82**, 123508 (2010), arXiv:0910.1066 [astro-ph.CO]
[39] S. Borsanyi *et al.*, Nature **539**, 69 (2016), arXiv:1606.07494 [hep-lat]
[40]
[41] 08(1)

SUPPLEMENTAL MATERIAL

Infinite volume extrapolation of fit parameters

In Fig. S1 we show the central values of the fit parameters ζ_0 and α_r (see Eq. 10) as well as the 1-σ uncertainties for $1k$, $2k$ and $4k$ simulations against $1/L$. The values can be seen in Tables II and III. As explained in the main text we perform a linear extrapolation to obtain the final results for ζ_0 and α_r, these linear extrapolations are shown in the plots as dashed lines.

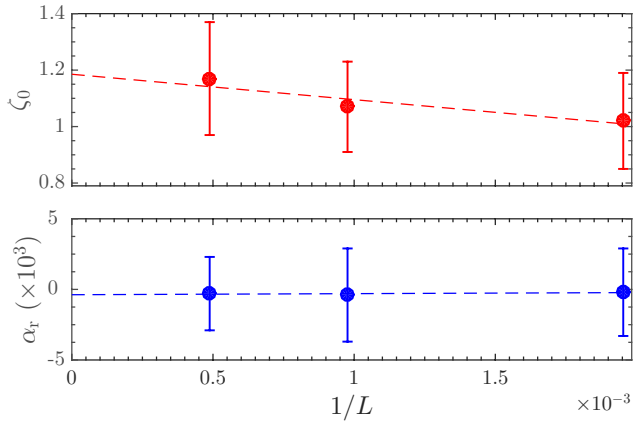

FIG. S1. Central values and estimated uncertainties of the fit parameters ζ_0 and α_r (see Tables II and III) plotted against $1/L$, where $L = N\delta x$ is the comoving side-length of the simulation box. The dashed lines are linear fits to the data points.

String separation and density from all simulations

In Fig. S2 we show plots of ξ against t and ζ against $\log(t\eta)$ for all simulations, where ξ is the mean string separation (3), ζ is the string length density parameter (4), t is cosmic time, and η the expectation value of the field. We additionally show two sets of $4k$ simulations with $k = 1008$, $\tau_{\rm ini}\eta = 70$, $\tau_{\rm diff}\eta = 90$, $\tau_{\rm cg}\eta = 307.4$, and $\tau_{\rm ini}\eta = 90$, $\tau_{\rm diff}\eta = 110$, $\tau_{\rm cg}\eta = 339.85$. These simulations were performed on a different architecture from the others, necessitating a slight reduction in the simulation volume. They are designed to confirm that ζ also tends to its scaling value from above in $4k$ simulations.

Dependence of fit parameters on initial conditions

In Fig. S3 we show the dependence of the fit parameters β, α^* and ζ_0^*, and α' and ζ_0' (6) on the fit parameter t_0/t_f, where t_0 is the time offset in the fit (5) and t_f is the end of the fitting period. The dotted line in the middle figure is Eq. (8), with t_f taken as the end of the fitting period (the rightmost dashed lines in Fig. S2). The solid black line represents our final result for the length density parameter (11) with the 1-σ variations represented as shaded regions.

Constant comoving width simulations

We also include the corresponding results for simulations with constant comoving width, i.e., using the Press-Ryden-Spergel method [34]: Table IV is analogous to Table II in the main text, i.e., it shows the central values and estimated uncertainties (as discussed in the main text after Eq. (5)) for β and $\zeta_0 = 1/4\beta^2$, but for simulations with constant comoving width. Also, the figures corresponding to Figs S2 and S3 are Figs. S4 and S5, respectively. The combined value for the length density parameter ζ_0 for the constant comoving width case is:

$$\zeta_0 = 1.34 \pm 0.22 \tag{13}$$

N	$\beta \pm \Delta\beta$	$\Delta\beta_{\rm stat}$	$\Delta\beta_{\rm sys}$	$\zeta_0 \pm \Delta\zeta_0$	$\Delta\zeta_{0,\rm stat}$	$\Delta\zeta_{0,\rm sys}$
$1k$	0.459 ± 0.040	0.040	0.027	1.21 ± 0.22	0.17	0.14
$2k$	0.447 ± 0.037	0.031	0.020	1.27 ± 0.21	0.18	0.12
$4k$	0.440 ± 0.035	0.029	0.020	1.31 ± 0.21	0.17	0.12

TABLE IV. Central values and estimated uncertainties of the standard scaling parameters β and $\zeta_0 = 1/4\beta^2$ for all box sizes for simulations with comoving string width. The decomposition into statistical and systematic uncertainties, as discussed in the main text after Eq. (5), is also shown.

Summary

Figs. S2, S3, S4 and S5 support our statements that:

1. Simulations which are scaling in the standard sense ($\xi \propto t$) have a slow evolution in the ζ - $\log(\eta t)$ plane.
2. Simulations converge to $\zeta \simeq 1$ from both above and below.
3. Convergence from below can look like a logarithmic increase in ζ, as observed in Refs. [24–27].
4. The coefficients of the logarithm and inverse logarithm have a strong dependence on the ratio t_0/t_f, consistent with their being a feature of the initial conditions.
5. The coefficients of the logarithm and inverse logarithm are consistent with zero at $t_0/t_f = 0$.
6. The constant terms in logarithm and inverse logarithm models are consistent with standard scaling at $t_0/t_f = 0$.

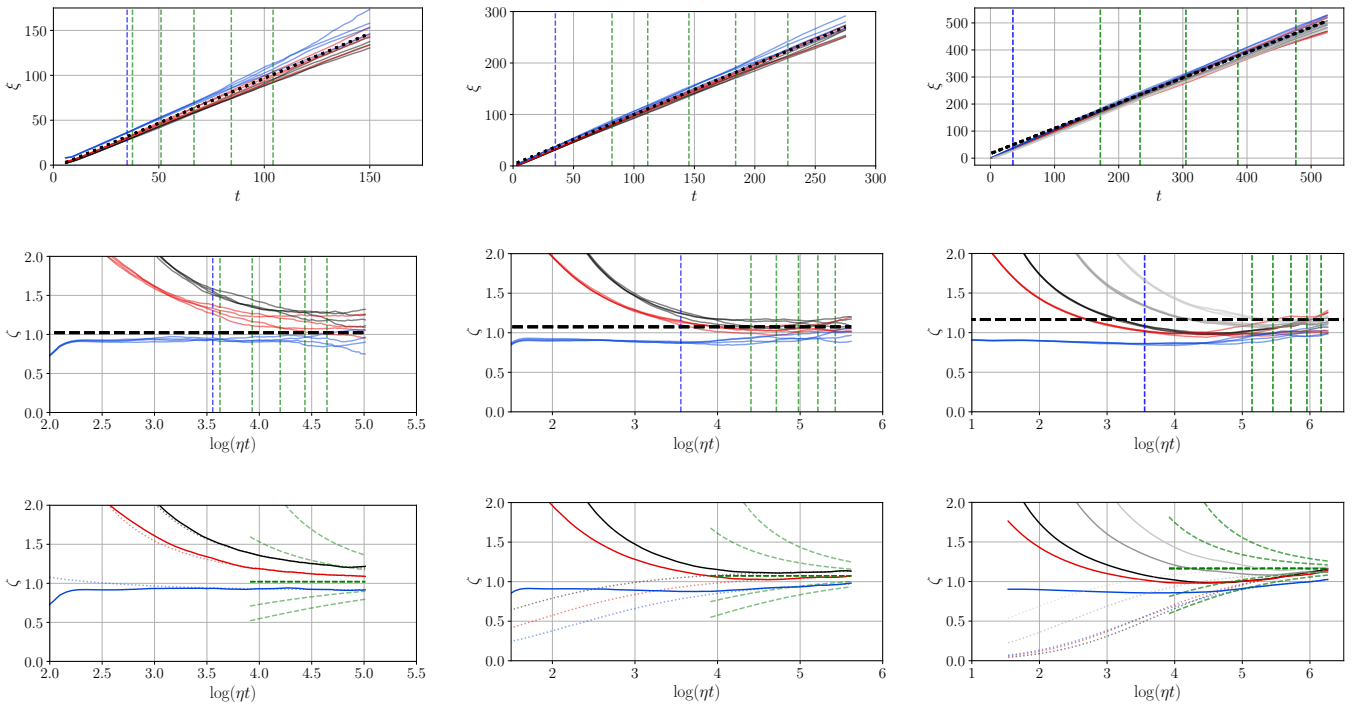

FIG. S2. We show data from the $1k$, $2k$ and $4k$ simulations from left to the right, where the black lines represent simulations with initial field correlation length $l_\phi = 5$, red ones with $l_\phi = 10$ and blue ones with $l_\phi = 20$. The $4k$ panel also contains an additional set of simulations with $l_\phi = 5$ and shifted initialisation times (see text for explanation) in grey. The blue vertical dashed lines are the end of the core growth period ($t_{\rm cg}$), after which strings maintain their physical width, and green ones are the boundaries of the fitting ranges. Top row: Mean string separation ξ (see Eq. 3) for each run simulated. The black dashed line represents $\xi = 2\beta(t - t_0)$, where β and t_0 are computed as stated in the main text for each lattice size. The values of β can be found in Table II. Middle row: The length density parameter ζ (see Eq. (4)) for each run. The black dashed lines represent $\zeta_0 = 1/4\beta^2$, where we used the values of β shown in Table II. Bottom row: The length density parameter ζ (see Eq. 4) averaged over the four runs with the same initial field correlation length l_ϕ. The dotted lines show the curves $\zeta = \zeta_0(1 - t_0/t)^2$, with the values of $\zeta_0 = 1/4\beta^2$ and t_0 used in figures at the top row. The green dashed lines are the fit curves $\zeta = \zeta_0(1 - t_0/t)^2$ with $\eta|t_0| = 0, 10, 20$.

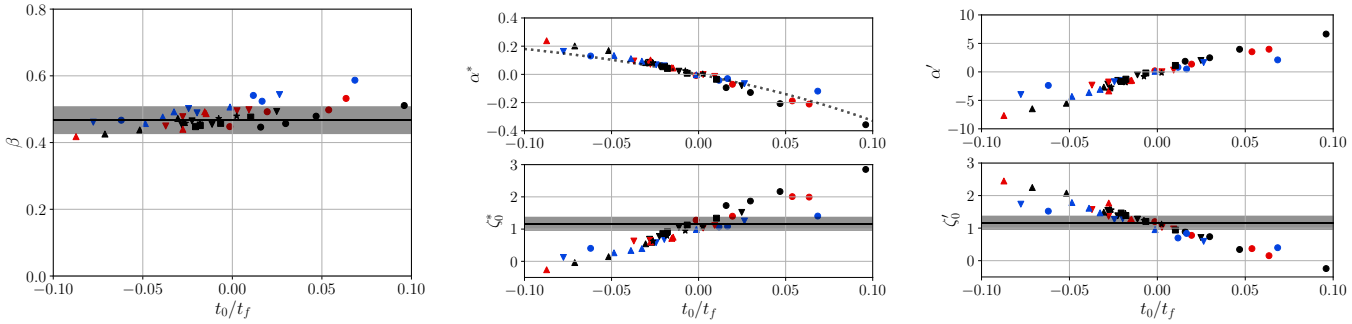

FIG. S3. Scatter plots showing the values of the fit parameters β (see Eq. 5) on the left, α^* and ζ_0^* in the middle, and α' and ζ_0' (see Eq. (6)) on the right, against t_0/t_f, where t_0 is the time offset in the fit (5), and t_f has been taken as the end of the fitting period (the rightmost dashed lines in Fig. S2). The black line with the shaded region in the leftmost figure represents $\beta = 1/2\sqrt{\zeta_0}$ with its 1-σ variation, where the value has been taken to be the one in Eq. (11) (i.e., $\zeta_0 = 1.19 \pm 0.20$). The black lines with the shaded region in the bottom of the other two figures are the corresponding ζ_0 with its 1-σ variation. The dotted line in the middle figure represents $\alpha^*(t_f) = -2\zeta(t_0/t_f)(1 - t_0/t_f)^{-1}$. The color code of the points represent the initial field correlation length where $l_\phi = 5$ is black, $l_\phi = 10$ is red and $l_\phi = 20$ is blue. $1k$ simulations are represented as circles, $2k$ simulations as triangles pointing downwards, $4k$ simulations as triangles pointing upwards and $4k$ simulations with shifted initialisation times as stars ($\tau_{\rm ini}\eta = 70$) and squares ($\tau_{\rm ini}\eta = 90$)

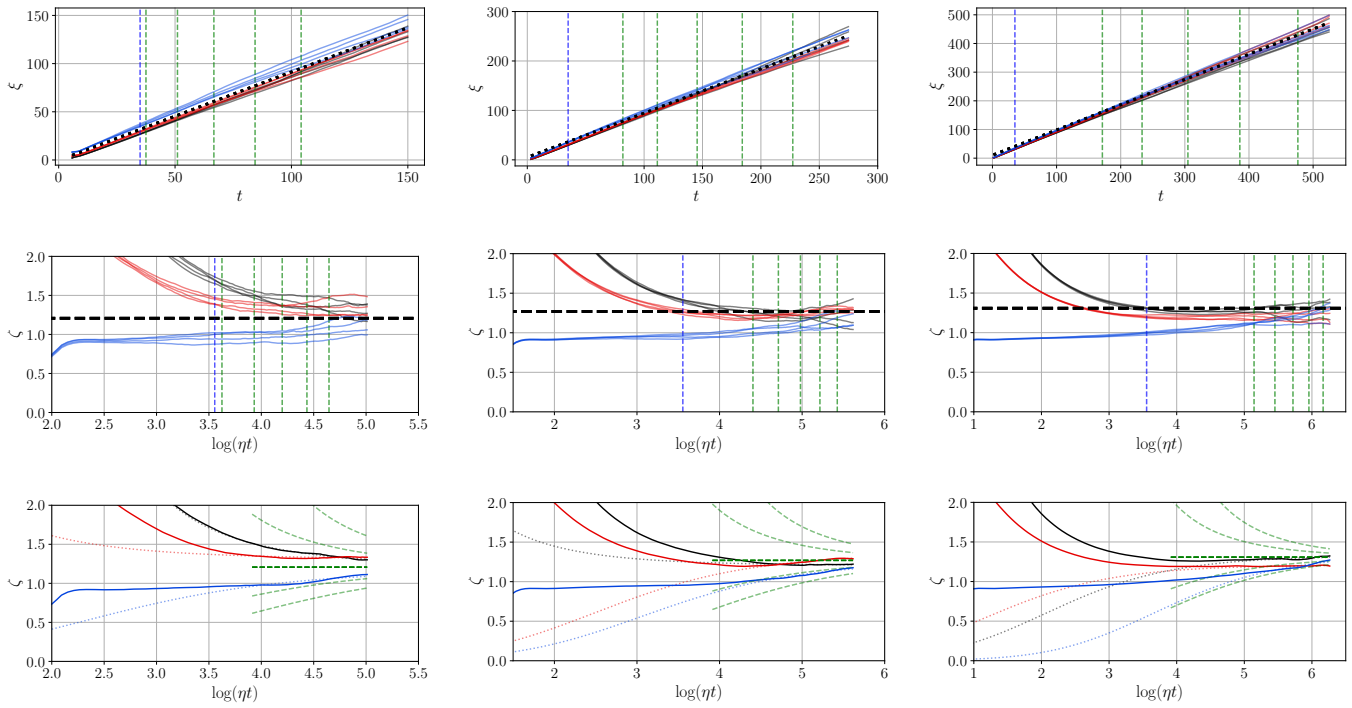

FIG. S4. As Fig. S2 but for simulations with constant comoving width. in this case, the values of β for the dashed lines in the figures in the top row, and for $\zeta_0 = 1/4\beta^2$ in the middle row can be found in Table IV.

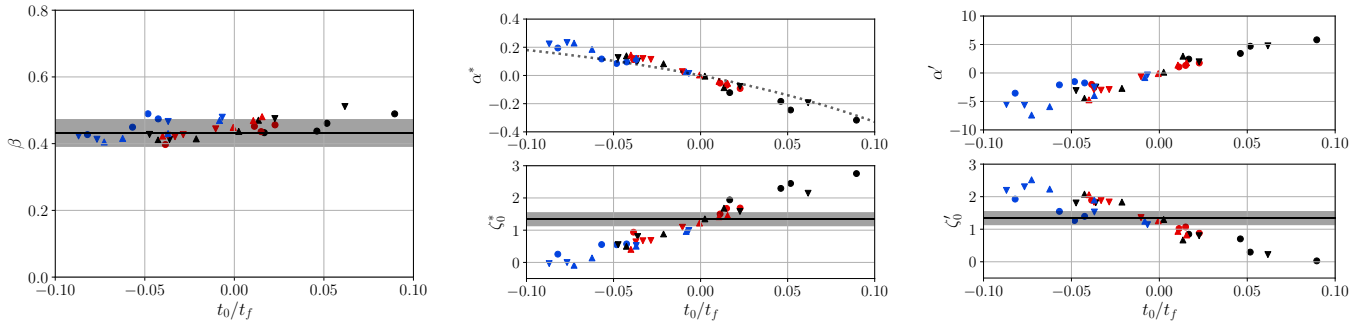

FIG. S5. As Fig. S3 but for simulations with constant comoving width. In this case, the black line with the shaded region in the leftmost figure also represents $\beta = 1/2\sqrt{\zeta_0}$ with its 1-σ variation, and the black lines with the shaded region in the bottom of the other two figures represent ζ_0 with its 1-σ variation; but the value used is the one in Eq. 13 (i.e., $\zeta_0 = 1.34 \pm 0.22$).